THE OHIO STATE UNIVERSITY

Models of polarized Lyman-α emission from cosmic ionization fronts and extraction of front parameters from 21cmFAST tool

By

Yuanyuan Yang

A THESIS SUBMITTED IN PARTIAL FULFILLMENT OF THE REQUIREMENTS FOR THE DEGREE OF

Bachelor of Science in Astronomy and Astrophysics

May 2022

SUPERVISOR

Christopher Hirata

ABSTRACT

The epoch of reionization is one main history of the universe, and it gives both cosmologists and astrophysicists insights into energy radiation, cosmic microwave background (CMB), galaxy formation, etc. Intensity mapping (IM) is one of the novel methods in probing the reionization, and Lyman-α forest is one of its main focuses. Thus, I want to study the epoch of reionization by looking at the Lyman-α emission from that period. In this paper, I present the formalism of simulating Lyman-α emission and polarization from a signal plane-parallel ionization front at redshift $z = 8$ and show the method of extracting needed parameters from the 21cmFAST tool. To build the model, I first use the Lyman-α emissivity to generate a Lyman-α photon from a presetting ionization front. Then I propagate the Lyman-α photon at a distance related to its mean free path and hit it with a hydrogen atom. The Lyman-α photon will scatter and repeat those steps until it hits either the boundary of the front of the frequency limit. After the Lyman-α photon hits the limits and escapes, I record its basic information, such as escaping position, direction, polarization, and frequency, for further calculation, such as the intensity, polarized intensity, and power spectrum of the front. The parameters for this model are blackbody temperature $T_{\rm bb}$, front velocity U, and number density of neutral hydrogen $n_{\rm H}$. To expand this model into coeval cubes, the model that contains all the information of the universe under a fixed time, generated by the 21cmFAST tool, as $T_{\rm bb}$ is set, I will calculate U and $n_{\rm H}$ from the coeval data boxes.

The source code can be found at https://github.com/SourceYang/Lyman-alpha

1 Introduction

Following the Big Bang, the universe expanded and cooled. At the time of recombination, the temperature dropped low enough for the hydrogen gas to transition from ionized to neutral. Later, when the first stars and galaxies formed, the ultraviolet radiation they produced led the hydrogen in the intergalactic medium to become reionized. The epoch of reionization is of broad interest for both cosmologists and astrophysicists. From the cosmologist's perspective, the ionization and thermal history of the Universe is key to studies of novel sources of energy injection [1] and dark matter physics [2]; it underlies studies of the power spectrum with the Lyman-α forest [3, 4]; and through its effect on the normalization of cosmic microwave background (CMB) anisotropies it affects studies of dark energy and modified gravity [5]. From the astrophysicist's perspective, reionization is interesting as a way of learning about the early sources of ionizing radiation [6–8], in its own right as a major event in the history of the intergalactic matter, and through its feedback effect on the formation of small galaxies [9].

We have several ways of probing the history and structure of reionization, and intensity mapping (IM) is one of the novel methods. Different from the traditional survey, intensity mapping collects and statistically analyses the emission line from galaxies and intergalactic medium, which can give information for a larger-scale and higher redshift universe, such as the epoch of reionization [10]. The large-scale polarization of the CMB due to Thomson scattering after reionization gives a global constraint and suggests that the midpoint of reionization occurred at redshift $z \approx 7.7 \pm 0.7$ [11]. Lyman-α absorption gives constraints on individual lines of sight, and is sensitive to neutral gas; even a small amount of H I can result in a deep absorption trough in the spectrum of a quasar or other source [12]. Such troughs are observed at $z \gtrsim 6$ [13, 14], although the interpretation is complicated by the modest number of sightlines and the fact that Lyman-α absorption saturates at even a small ($\sim 10^{-4}$) neutral fraction [15]. One can also probe reionization using Lyman-α

emitters (LAEs) since neutral gas in the IGM can scatter Lyman-α photons out of the line of sight; thus LAEs can provide insights into the history and structure of reionization [16–19]. In the near future, it may be possible to map neutral hydrogen during the reionization epoch using H I 21 cm emission [20, 21]. This is a faint line, and the foreground challenges in this part of the radio spectrum are significant, but the 21 cm line is optically thin at IGM densities and it does not require a background source.

One of the ways we hope to learn about reionization is through the Lyman-α emission from galaxies in that epoch. Lyman-α is a spectral line of hydrogen with a wavelength of 1216 Å. We focus on spectral lines of hydrogen because it is the most abundant element in the universe. The Lyman-α line also has immense diagnostic power because when a Lyman-α photon encounters a hydrogen atom, it scatters instead of being destroyed. Therefore, when we observe Lyman-α, we can see neutral gas, which is otherwise invisible, by looking at the scattered light.

Because Lyman-α photons scatter off of even small column densities of H I, we might expect it to be linearly polarized, and for this polarization to encode important geometrical information since the most likely direction of polarization is perpendicular to the plane of the last scattering. Prior to reionization, we expect a source to be surrounded by a "halo" of scattered, polarized Lyman-α light [22]; this may be modified depending on the local velocity structure of the H I around the source [23]. There is one detailed study so far of the polarization power spectrum of Lyman-α in the reionization epoch [24], which focused on scattered radiation from galaxies. On larger scales, however, we might expect the ionization fronts themselves to contribute significantly to the polarized intensity mapping signal. Cosmological ionization fronts are warm and partially ionized, so they should cool by Lyman-α emission from collisionally excited H I [25, 26], and due to multiple scattering, this radiation should be polarized when it emerges from the front. The direction of polarization should be related to the orientation of the ionization front. Moreover,

ionization bubbles are coherent over large scales (likely tens of cMpc), and thus are a good candidate for contributing to the power spectrum at large scales. Detection of this signal with future instruments could in principle be an interesting diagnostic of the geometrical structure of reionization.

In this paper, I will create a model for simulating Lyman-α emissions from reionization in a single plane-parallel ionization front. This includes generating, propagating, and scattering Lyman-α photon processes, and will predict the final status, especially the intensity and polarization of Lyman-α radiation. Looking forward, I want to extend this to a cosmological simulated ionization front and extract the needed parameters from the simulating data.

2 Ionization Front Models

The fiducial model is based on the ionization front (I-front) of Zeng et al. [27] at redshift $z = 8$. The ionization front velocity $U = 5 \times 10^8$ cm s^{-1}, and incident radiation with a blackbody spectrum at temperature $T_{\rm bb} = 5 \times 10^4$ K. It separates the I-front into $N_{\rm grid} = 2000$ slabs, and each slab has physical width $N_{\rm H}/n_{\rm H}$ (unit: cm), where $N_{\rm H}$ (unit: cm^{-2}) is the column density of hydrogen (in all forms: neutral or ionized) and $n_{\rm H}$ (unit: cm^{-3}) is the total number density of hydrogen.

In this paper, I want to simulate a range of I-front parameters so that the results can be pasted onto a cosmological simulation. I simulate ionization front speed U from $5{\times}10^7$ cm s^{-1} to $5{\times}10^9$ cm s^{-1}, incident radiation temperature $T_{\rm bb}$ from $5{\times}10^4$ K to 10^5 K, and $n_{\rm HI}$ from $1.37{\times}10^{-5}$cm^{-3} to $1.37{\times}10^{-3}$cm^{-3} (i.e., 0.1 to 10$\times$ mean density at $z = 8$).

I find that in my simulations, it is possible for a photon in the damping wings of the Lyman-α line to travel far into the neutral side of the front, and then re-scatter. To account for this possibility, I set $N_{\rm grid} = 2 \times 10^5$.

One aspect of the Zeng et al. [27] simulations that I have changed for this paper is the initial temperature. For thermal evolution of the ionization front, it is sufficient to start from idealized "cold" initial conditions with temperature very near zero. However, for radiative transfer calculations, very low temperatures lead to very narrow Doppler widths and very short length scales for a photon to redshift through a line, which is challenging for this numerical method. For this paper, I used the temperature $T_{\rm i} = 1.7454197377$ K based on standard cosmological recombination and Compton de-coupling [28], with no additional heating sources such as X-ray heating.

I use the variable Z from 0 to $2 \times 10^5 - 1$ to express the position of the Lyman-α photon. Here $Z = 0$ is the ionized side with smaller $N_{\rm HI}$ and $Z = 2 \times 10^5 - 1$ is the neutral side with higher $N_{\rm HI}$.

I use the cosmological model from *Planck* 2018 results [11]: $H_0 = 67.4$ km s^{-1}Mpc^{-1}, $\Omega_{\rm m} = 0.315$, $\Omega_\Lambda = 1 - \Omega_{\rm m} = 0.685$, and $\Omega_{\rm b} = 0.0224/h_0^2$, where h_0 is current Hubble constant divided by 100 km s^{-1}Mpc^{-1}.

3 Method: Monte Carlo

After finishing setting the background front, I start to simulate the production, propagation, and escape of Lyman-α photons. I track several properties of the photon:

- The position Z (measured in the sense that positive is toward the neutral side).
- The frequency offset $\Delta\nu = \nu - \nu_{{\rm Ly}\alpha}$ (measured so that $\Delta\nu > 0$ on the blue side of the line and $\Delta\nu < 0$ on the red side of the line).
- The direction of propagation $\mu = \cos\theta$ (measured so that $\mu = +1$ is toward the neutral side and $\mu = -1$ is toward the ionized side).

- The linear polarization $p = Q/I$ (measured so that $p = +1$ is polarized in the North-South plane containing the z-direction, and $p = -1$ is polarized in the East-West plane perpendicular to the z-direction).

Since the ionization front model is plane-parallel, I do not need to track the x or y coordinate of the photon or the longitude ϕ of the propagation direction; and the diagonal (U/I) and circular (V/I) polarization of the photon are zero by symmetry.

To begin the simulation of each photon, I place a photon at a position drawn from the emissivity distribution, give it an isotropic initial direction and polarization, and set its initial frequency based on the Voigt profile. Then I propagate the photon based on its mean free path until it hits a hydrogen atom and scatters, or escapes from the simulation grid. I describe the details of generating a photon in §3.1, propagation in §3.2, and scattering in §3.3. Figure 1 is the flowchart of the whole Monte Carlo process.

3.1 Generate a Photon

In order to generate a particular Lyman-α photon, I need the initial position, frequency, direction, and polarization of the photon.

I start with generating a photon at a position Z with a probability given by the distribution of Lyman-α emissivity. The Lyman-α emissivity, which means the number of Lyman-α photons emitted per unit volume per unit time (unit: $\mathrm{cm^{-3}\ s^{-1}}$), is given by

$$\frac{dN}{dV\,dt} = n_\mathrm{e} n_\mathrm{HI} q_{\mathrm{Ly}\alpha}(T_\mathrm{e}), \tag{3.1}$$

where n_e (unit: $\mathrm{cm^{-3}}$) is the electron density, and $q_{\mathrm{Ly}\alpha}$ (unit: $\mathrm{cm^3\ s^{-1}}$) is the rate coefficient for hydrogen excitation,

$$\mathrm{H(1s)} + e^- \ \rightarrow\ \mathrm{H(nl)} + \mathrm{e^-}, \tag{3.2}$$

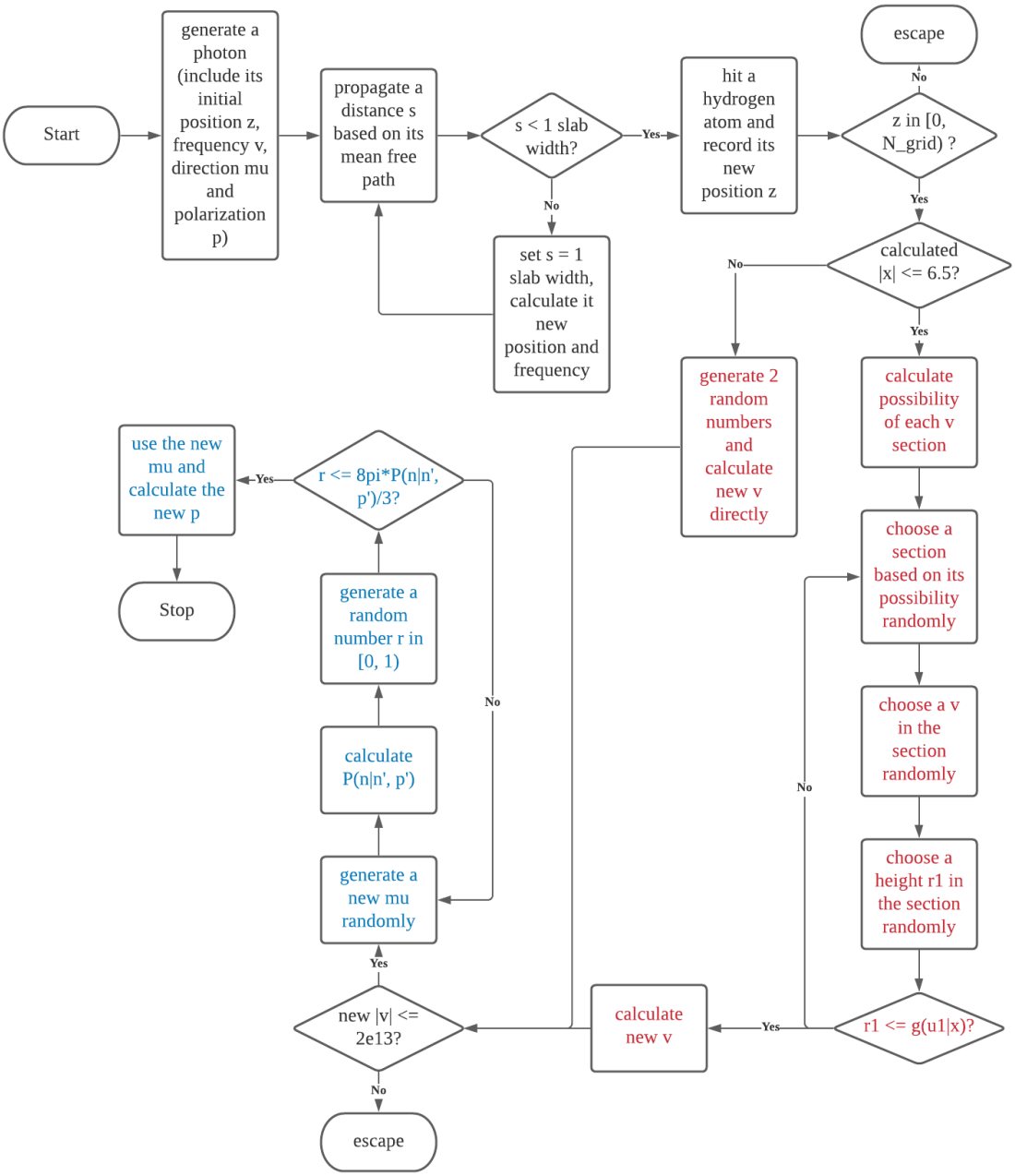

Figure 1: Flowchart of the Monte Carlo method

given in Aggarwal [29]. I include the low-lying excitations to 2p, 3s, and 3d, since decays from these levels lead to Lyman-α emission. Excitation to 2s leads to 2-photon continuum emission. Excitation to 3p leads to Hα+2 photon continuum emission under conditions with high optical depth, so is not included here. Excitation

to $n \geq 4$ levels can lead to Lyman-α with some small probability [30, 31], but is not included here because the excitation rates will in any case be smaller than $n = 2$ or 3.

The aforementioned calculation gives the emission rate in each slab. The cumulative probability for a photon to be generated in slab number $\leq i$ is

$$P_i = \frac{\sum_{i'=0}^{i} (dN/dV\, dt)_{i'}}{\sum_{i'=0}^{N_{\rm grid}-1} (dN/dV\, dt)_{i'}}. \tag{3.3}$$

I generate a uniform random number ξ from 0 to 1, and assign it to the slab i where $P_{i-1} \leq \xi < P_i$. Within each slab, we assign a random position, i.e., the initial position Z is uniform between i and $i+1$. The total emissivity in the ionization front model converges because on the ionized side, the H I density declines exponentially (atoms exposed to the incident UV flux are ionized); and on the neutral side, the temperature declines and the excitation rate $q_{\rm Ly\alpha}$ is exponential in temperature. Figure 4a is an example of generated position.

For the initial direction, I choose an isotropic distribution, i.e., the direction cosine $\mu = \cos\theta$ is uniformly chosen between -1 and $+1$. Then set initial polarization is $p = 0$. These are appropriate choices for electron impact excitation from a locally thermalized (hence isotropic) distribution of electrons.

Finally, it comes to the frequency. The frequency of Lyman-α emission corresponds to Voigt distribution, which is

$$\Phi(\Delta\nu) = \int_{-\infty}^{\infty} d\Delta\nu' \Phi_{\rm G}(\Delta\nu') \Phi_{\rm L}(\Delta\nu - \Delta\nu') \tag{3.4}$$

where $\Delta\nu = \nu - \nu_{\rm Ly\alpha}$ (unit: Hz) is the frequency offset from $\nu_{\rm Ly\alpha}$, and $\nu_{\rm Ly\alpha}$ (unit: Hz) is the center frequency of Lyman-α emission line. The Gaussian component due to thermal motion of the atoms is

$$\Phi_{\rm G}(\Delta\nu) = \frac{1}{\sqrt{2\pi}\,\sigma} e^{-\Delta\nu^2/(2\sigma^2)}, \quad \sigma = \frac{\nu_{\rm Ly\alpha}\sqrt{kT_{\rm HI}/m_{\rm HI}}}{C}, \tag{3.5}$$

and the Lorentzian component due to natural broadening of the 2p level is

$$\Phi_{\rm L}(\Delta\nu) = \frac{\gamma}{\pi(\gamma^2 + \Delta\nu)^2}, \quad \gamma = \frac{1}{4\pi T_{\rm 2p}}. \tag{3.6}$$

Here k (unit: g cm^2 s^{-2} K^{-1}) is Boltzmann's constant, $T_{\rm HI}$ (unit: K) is the temperature of the neutral hydrogen atoms, $m_{\rm HI}$ (unit: g) is the mass of hydrogen atom, C (unit: cm s^{-1}) is the speed of light, and $T_{\rm 2p}$ (unit: s) is the lifetime of H(2p).

Since the total line profile Φ is a convolution of the two terms, it can be computed by adding a Gaussian random variable to a Lorentzian random variable, $\Delta\nu = \nu_{\rm G} + \nu_{\rm L}$. I generate the Gaussian random variable by the polar transformation method, and the Lorentzian by a univariate transformation method (since the inverse of the cumulative distribution function can be solved analytically).

3.2 Propagate a Photon

After getting the initial status of a Lyman-α photon and before the photon is absorbed by a hydrogen atom, this photon will propagate through the space. In order to calculate the average distance the photon moved before it interacts, I want to calculate the mean free path ($\ell_{\rm mfp}$, unit: cm) of the photon:

$$\ell_{\rm mfp} = \frac{1}{n_{\rm HI}\sigma_{\rm tot}} \tag{3.7}$$

The $n_{\rm HI}$ here is the number density of neutral hydrogen, which is calculated by the initial hydrogen density times the neutral fraction of hydrogen in the slab. The total cross section $\sigma_{\rm tot}$ (unit: cm^{-2}) generally includes all processes, but in our frequency range only the Lyman-α transition (1s$\rightarrow$2p) is important; it is

$$\sigma_{\rm tot}(\Delta\nu) = \frac{3A\lambda_{\rm Ly\alpha}^2}{8\pi}\phi(\Delta\nu) \tag{3.8}$$

where A (unit: s^{-1}) is the spontaneous decay rate for the transition from 2p to 1s, $\lambda_{\rm Ly\alpha}$ (unit: cm) is the wavelength of the Lyman-α photon, which will be finally transferred into frequency, and $\phi(\Delta\nu)$ is the Voigt probability distribution.

The calculation of Voigt distribution is somewhat complicated, my calculation uses the series expansion in the Voigt parameter [32] to second order (H_2 term). For the Dawson integral $F(x)$ that appears in the first order (H_1) term, I separate it into two

cases: the small $|x|$ case and the large $|x|$ case, where $x = \Delta\nu/\sqrt{2}\sigma$ is the frequency offset parameter. For $|x| < 8$, I use the Taylor expansion, and for $|x| > 8$ I use the asymptotic expansion. The Taylor expansion of the Dawson integral is given by

$$F(x) = \sum_{n=0}^{14} \frac{(-1)^n 2^n}{(2n+1)!!}(x^{2n+1}) \tag{3.9}$$

and the asymptotic solution is given by

$$F(x) = \sum_{n=0}^{x^2+10|x|} 2^{-n-1} x^{2n-1} (2n-1)^n. \tag{3.10}$$

The numerical calculation of $F(x)$ is at least accurate to 14 digit places at the matching point $|x| = 8$.

From the mean free path, I can generate the travel distance s of the photon from an exponential distribution of mean $\ell_{\rm mfp}$. As the ionization front is also moving, the photon moves $\Delta s = s\mu - Us/C$ relative to the ionization front. Finally, I divided the Δs by the width of the slab to convert it to the slab-based system. To account for the universe expanding and therefore the photon redshifting, the frequency of the Lyman-α photon will be reduced according to

$$\Delta\nu_{\rm new} = \Delta\nu_{\rm old} - H(z)s\frac{\Delta\nu + \nu_{\rm Ly\alpha}}{C}, \tag{3.11}$$

where

$$H(z) = H_0\sqrt{\Omega_m(1+z)^3 + \Omega_\Lambda} \tag{3.12}$$

is the Hubble constant (unit: $\rm s^{-1}$) at the epoch of redshift $z = 8$.

One complication is that in an inhomogeneous Universe, the mean free path $\ell_{\rm mfp}$ is spatially variable and the propagation distance is not exponentially distributed. I solve this by clipping the exponential distribution: if the photon enters the next slice, its position is reset to the boundary between slices, I compute the distance s traveled before the photon reaches the boundary, and update the frequency according to Eq. (3.11). I then re-propagate the photon in the same direction. The same clipping procedure is also applied if the photon propagates a distance s larger than or equal to

1 slab width; this is especially important if the propagating direction is near parallel to the front, since then it may change its frequency significantly before it hit a slab boundary.

3.3 Scattering a Photon

After the Lyman-α photon moved a certain distance and was absorbed by a hydrogen atom, it will scatter rather than be destroyed and will have a new frequency, direction, and polarization. In this section, I will describe how to get those new properties step by step. This first involves solving for the velocity of the atom that causes the scattering, and then it involves drawing the outgoing direction (and hence frequency) and polarization in the I-front frame.

I use the rejection method based on Lee's paper [33] to calculate the frequency redistribution of the Lyman-α photon. Before getting started, I want to introduce the transverse velocity of the atom. Based on Lee's work, I decompose the velocity of the atom into two components: along with observers' direction's velocity v_1 and perpendicular to observers' direction's velocity v_2. By applying a normalization factor, I introduce two transverse velocities: $u_1 = \sqrt{m/2kT}v_1$ and $u_2 = \sqrt{m/2kT}v_2$. I will redistribute u_1 and u_2 separately, then calculate them into x, as well as the $\Delta\nu$ I wanted.

First, I redistribute u_1. When $|x| \geqslant 6.5$, I choose two random numbers r_1 and r_2 between 0 and 1, then $u_1 = 1/x + \sqrt{-\log(r_1)}\cos(2\pi r_2)$. I modify the derivation for u_1 when $|x| < 6.5$. To use the rejection method, I want to build a region with 3 rectangles, where the horizontal endpoints are u_{1a} = -7, u_{1b} = x - 0.25, u_{1c} = x + 0.25 and u_{1d} = 7. I ignore the cases that are outside this range because the probability of being outside is about 4.5×10^{-19}, which is negligible. For the height of each rectangle, I want to use the largest value of each section, and there are two cases. When the $|x| < 2$, the largest values happen at the endpoints and I compare the two endpoint values $\exp(-u_1^2)/(u_1 - x)^2$ then choose the larger one. While when

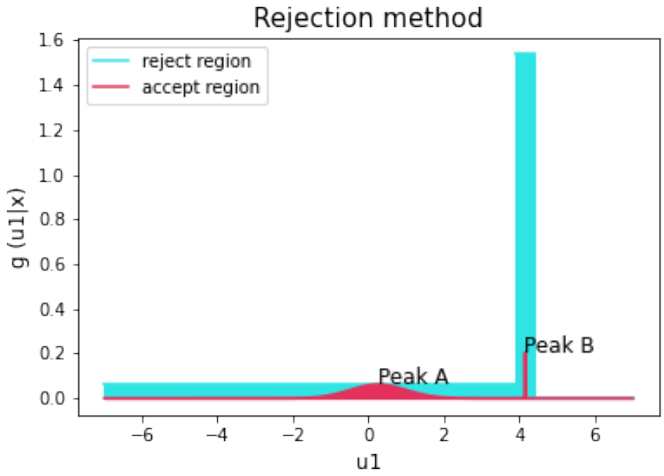

Figure 2: Sample of rejection region and accept region when $x = 4.14$

$|x| > 2$, we need to set a midpoint $u_{1e} = (x - \text{sign}_x\sqrt{x^2 - 4})/2$, and compare its $\exp(-u_{1e}^2)/(u_{1e} - x)^2$ to others and choose it if it any larger. After getting the width and height of each rectangle, I can compute the areas of them. Then I can compute the fraction of each area, which is also the probability of each region for a Lyman-α photon to select. Thus, in the rejection method, I can firstly use a random number to choose a rectangle, then use two random numbers to choose a point in that rectangle, and finally, test whether the point is under the curve $g(u_1|x)$ with corresponding u_1. I use a while loop to accept the u_1 if it is under the curve and redo the whole process again if not. Figure 2 is a sample of rejection method with rejection area and accept area when $x = 4.14$. Second, I redistribute u_2, which is simply $\sqrt{-\log(r_1)}\cos(2\pi r_2)$, where r_1 and r_2 are two random numbers between 0 and 1.

Then, I want to calculate the new direction and polarization for the Lyman-α photon together as these two properties are dependent. I start with the new direction, and setting six angles θ, θ', α, β, γ and ζ which are shown in the Figure 3. The angle θ' is the initial direction, θ is the final direction, α is randomly chosen between 0 and 2π

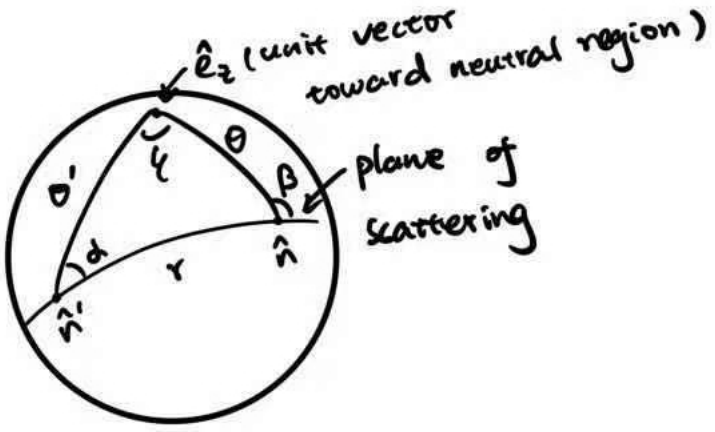

Figure 3: Angles for calculating the new direction

and $\cos\gamma$ is uniformly distributed between -1 and $+1$. From spherical trigonometry:

$$\begin{aligned}
\cos\theta &= \cos\theta'\cos\gamma + \sin\theta'\sin\gamma\cos\alpha, \\
\sin\theta\sin\beta &= \sin\theta'\sin\alpha, \\
\sin\theta\cos\beta &= \sin\theta'\cos\alpha\cos\gamma - \cos\theta'\sin\gamma, \\
\sin\theta\sin\zeta &= \sin\alpha\sin\gamma, \quad \text{and} \\
\sin\theta\cos\zeta &= \sin\theta'\cos\gamma - \cos\theta'\cos\alpha\sin\gamma,
\end{aligned} \tag{3.13}$$

and I can use rectangular-to-polar conversion to get θ, β and ζ individually. After getting each of those angles, I try to calculate the new polarization. The fractional linear polarization p is defined by

$$p = \frac{I_{\mathrm{NS}} - I_{\mathrm{EW}}}{I_{\mathrm{NS}} + I_{\mathrm{EW}}}, \tag{3.14}$$

where I_{NS} and I_{EW} means the intensities are measured in the North-South or East-West plane with the z-axis. This will always be between -1 and $+1$, with -1 indicating pure East-West polarization, $+1$ indicating pure North-South, and 0 unpolarized. Then the probability distribution for scattering from direction $\boldsymbol{n'}$ and polarization state q′ to direction $\boldsymbol{n}$ and polarization state q is

$$\mathrm{P}(\boldsymbol{n}, q|\boldsymbol{n}', q') = \frac{1 - E_1}{8\pi} + \frac{3}{8\pi} E_1 \cos^2\psi_{q,q'} \tag{3.15}$$

where $\psi_{q,q'}$ is the angle between the initial and final polarization directions, and E_1 indicates the scattering angular distribution [34]: $E_1 = 0$ indicates the pure isotropic scattering and $E_1 = 1$ indicates the pure dipole scattering. The value of E_1 depends on the angular momentum of the lower and upper levels.

In this case, the admixture of isotropic versus dipole scattering depends on the frequency and the fine and hyperfine structure of the atom. The scattering process is of the form

$$\mathrm{H}(1\mathrm{s}_{1/2}, F_\mathrm{i}) + \gamma \to \mathrm{H}(2\mathrm{p}_{j_\mathrm{e}}, F_\mathrm{e}) \to \mathrm{H}(1\mathrm{s}_{1/2}, F_\mathrm{f}) + \gamma, \tag{3.16}$$

where F_i, F_e, and F_f are the total angular momenta of the initial, excited, and final states, respectively. There is interference between the possible intermediate states ($j_\mathrm{e} = \frac{1}{2}$ and $\frac{3}{2}$, and $F_\mathrm{e} = j_\mathrm{e} \pm \frac{1}{2}$) [30]. I assume that the hydrogen atoms start with nearly random electron and nuclear spin, which is likely to be true in practice since all relevant temperatures are large compared to the hyperfine splitting ($k_\mathrm{B} \times 68$ mK). The problem simplifies in the case where the Voigt parameter $a \ll 1$ (natural width small compared to Doppler width), which is the case here. As can be seen from Figure 2, scattering events can be either off resonance (Peak A) or on resonance (Peak B).

For events that are *off-resonance*, the frequency denominators $1/(E_\mathrm{i} + h\nu - E_\mathrm{e})$ in the scattering amplitude are essentially the same for all intermediate states. In this case, the electron and nuclear spin degrees of freedom are spectators, so the angular distribution is appropriate for angular momentum $0 \to 1 \to 0$ scattering, i.e., $E_1 = 1$. For events that are *on-resonance*, we find the averaged angular distribution parameter over the set of resonances, $\int \phi(\nu) E_1(\nu)\, d\nu$, and average over initial states with 1:3 weighting of $F_\mathrm{i} = 0$ vs. $F_\mathrm{i} = 1$ ([30], Appendix B; note that there $\varpi_2 = \frac{1}{10} E_1$ is used instead). This yields $E_1 = \frac{1}{3}$ (in the limit that lines D and E coincide). I implement this behavior in the code by setting

$$E_1 = \begin{cases} 0 & |x - u_1| \le \sqrt{3}\, a \\ 1 & \text{else.} \end{cases} \tag{3.17}$$

This way, in the off-resonance region, I have $E_1 = 1$, but in the on-resonance region, I have E_1 either equal to 0 or 1, with an average of $\frac{1}{3}$ taken over the Lorentzian distribution.

I can now write the probability distribution for each of the two final polarization states (NS or EW), for a partially polarized incident photon (arbitrary p'):

$$\mathrm{P}(\boldsymbol{n}, \mathrm{NS}|\boldsymbol{n}', p') = \frac{1 - E_1}{8\pi} + \frac{3}{16\pi} E_1[(1 + p') \cos^2 \psi_{\mathrm{NS,NS}} + (1 - p') cos^2 \psi_{\mathrm{NS,EW}}] \quad (3.18)$$

and

$$\mathrm{P}(\boldsymbol{n}, \mathrm{EW}|\boldsymbol{n}', p') = \frac{1 - E_1}{8\pi} + \frac{3}{16\pi} E_1[(1 + p') \cos^2 \psi_{\mathrm{EW,NS}} + (1 - p') \cos^2 \psi_{\mathrm{EW,EW}}]. \quad (3.19)$$

The angles can be inferred from spherical trigonometry; the explicit expressions are

$$\begin{aligned} \cos \psi_{\mathrm{NS,NS}} &= \sin\theta \sin\theta' + \cos\theta \cos\theta' \cos\zeta, \\ \cos \psi_{\mathrm{NS,EW}} &= -\cos\theta \sin\zeta, \\ \cos \psi_{\mathrm{EW,NS}} &= \cos\theta' \sin\zeta, \quad \text{and} \\ \cos \psi_{\mathrm{EW,EW}} &= \cos\zeta. \end{aligned} \quad (3.20)$$

The total probability is

$$\mathrm{P}(\boldsymbol{n}|\boldsymbol{n}', p') = \mathrm{P}(\boldsymbol{n}, \mathrm{NS}|\boldsymbol{n}', p') + \mathrm{P}(\boldsymbol{n}, \mathrm{EW}|\boldsymbol{n}', p'). \quad (3.21)$$

As the probability $\mathrm{P}(\boldsymbol{n}|\boldsymbol{n}', p')$ has a maximum possible value of $3/(8\pi)$, I also use the rejection method here. I will generate a random number between 0 to 1, and accept the process if the random is smaller than $(8\pi/3)\mathrm{P}(\boldsymbol{n}|\boldsymbol{n}', p')$, and otherwise draw again. The final polarization for that photon should be given by the relative probabilities to scatter into the NS or EW state, then the final polarization p is

$$p = \frac{\mathrm{P}(\boldsymbol{n}, \mathrm{NS}|\boldsymbol{n}', p') - \mathrm{P}(\boldsymbol{n}, \mathrm{EW}|\boldsymbol{n}', p')}{\mathrm{P}(\boldsymbol{n}, \mathrm{NS}|\boldsymbol{n}', p') + P(\boldsymbol{n}, \mathrm{EW}|\boldsymbol{n}', p')}. \quad (3.22)$$

The algorithm to get the redistributed direction and polarization is thus:

1. Generate two random angles α and γ, then calculate θ, β, and ζ;
2. calculate E_1;
3. calculate the angles $\psi_{\mathrm{NS,NS}}$, $\psi_{\mathrm{NS,EW}}$, $\psi_{\mathrm{EW,NS}}$, $\psi_{\mathrm{EW,EW}}$, and then calculate the probability densities $\mathrm{P}(\boldsymbol{n}, \mathrm{NS}|\boldsymbol{n}', p')$ and $\mathrm{P}(\boldsymbol{n}, \mathrm{EW}|\boldsymbol{n}', p')$;
4. calculate the total probability $\mathrm{P}(\boldsymbol{n}|\boldsymbol{n}', p')$;
5. generate a random number between 0 to 1, if the random number is smaller than $(8\pi/3)P(\boldsymbol{n}|\boldsymbol{n}', p')$, go next step, otherwise go back to step 1;
6. calculate p; and then
7. the final direction is θ, and the final polarization is p.

After getting scattering velocity and direction, I can calculate the new frequency offset (in Doppler units) x, which is

$$x_{\mathrm{new}} = x_{\mathrm{i}} + u_1 \cos\gamma + u_2 \sin\gamma - u_1. \tag{3.23}$$

Multiplying by the local Doppler width, I get the new frequency offset $\Delta\nu = \sqrt{2}\,\sigma x$.

4 Model Tests

In order to guarantee the model runs correctly, it needs to test the code step by step.

4.1 Photon generation

To begin with, I test the photon generating process, starting with testing the position generating process.

Figure 4a shows the distribution of the generated position of photons. The initial position test runs 10^6 photons under the setting of blackbody incident temperature

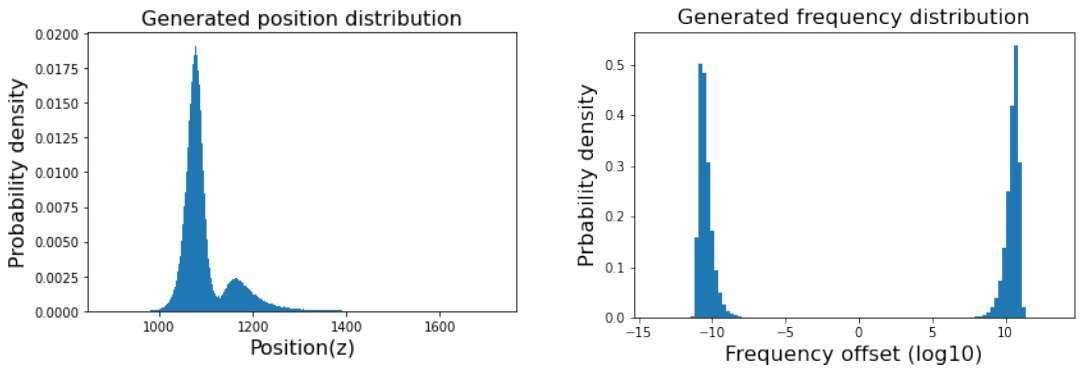

(a) (b)

Figure 4: Distribution of generated position (a) and frequency (b)

$T_{\rm bb} = 5 \times 10^4$K, ionization front velocity $u = 5 \times 10^8$cm s^{-1}, and front hydrogen density $n_{\rm HI} = 1.37 \times 10^{-4}\,{\rm cm}^{-3}$. As the ionized side has no neutral hydrogen atom to excite and the neutral side has almost no electrons and is very cold, the Lyman-α emissivity should be zero on either side, as seen. In this figure, most of the Lyman-α photons emitted at slice number $Z \approx 1100$, where the ionization fraction of hydrogen first reaches 0.5, which matches what I expected. The second peak is a result of $T_{\rm e}$ being larger than on the ionized side [27]; this is expected because of the exponential dependence of the excitation rate coefficients.

Secondly, I test the frequency generator. Figure 4b shows the distribution of the generated frequency of photons. This test runs 10^6 photons under the setting of background temperature of hydrogen atom $T_{\rm HI} = 5000$ K. The Doppler width σ in Eq. (3.5) is about 5.29×10^{10} Hz. Thus, the absolute value of generated $\Delta\nu$ is expected to be around 10^{10} Hz. The distribution corresponds to the expectation.

4.2 Photon propagation

Here I test the propagating process. In order to do this test more precisely, I test both propagation toward the neutral side ($\mu > 0$) and toward the ionized side ($\mu < 0$). Figure 5 shows two cases: (a) $\Delta\nu = 10^{10}$ Hz, $\cos\theta = 0.5$ and $T_{\rm HI} = 20000$K;

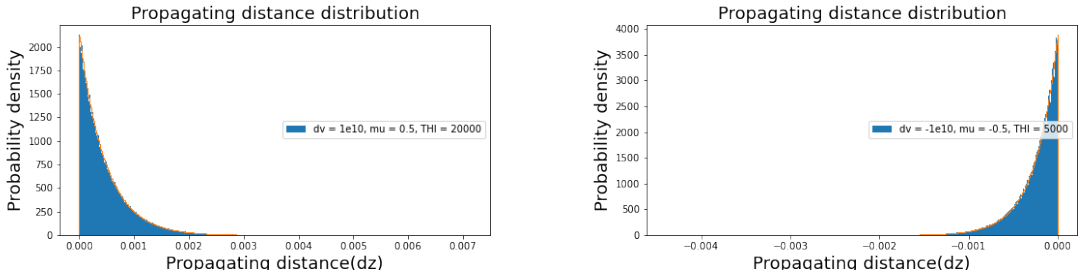

(a) (b)

Figure 5: Distribution of propagation distances (projected onto the z-axis): (a) toward the neutral side and (b) toward the ionized side. In both cases, the distribution follows the expected exponential distribution.

and (b) $\Delta\nu = -10^{10}$ Hz, $\cos\theta = -0.5$ and $T_{\rm HI} = 5000$K. Each test runs 10^7 photons. The orange line shows the theoretical distribution calculated corresponding to Section 3.2, and it is consistent with the simulation results.

4.3 Scattering frequency

To test the scattering process, I need to test the scattering frequency, scattering direction, and scattering polarization results. I start with the scattering frequency tests. Note that the scattering frequency test generally uses the normalized frequency offset x and projection of the atom velocity along the incoming photon direction u_1, rather than $\Delta\nu$.

To test the selection of scattering atom velocity, I test the Gaussian (larger $|x|$) conditions, Lorentzian (smaller $|x|$) conditions, and the combination of Gaussian and Lorentzian (middle $|x|$) limiting cases for $\mathrm{P}(u_1|x)$. Figure 6a shows the Gaussian limit with $\Delta\nu = -10^{12}$ Hz and $T_{\rm HI} = 12000\,\mathrm{K}$; here $x = 8.627$, the incoming photon is in the red damping wing of the Lyman-α line, and $\mathrm{P}(u_1|x)$ is a small perturbation on the Maxwellian distribution $\propto e^{-u_1^2}$. Figure 6b shows the Lorentzian limit with $\Delta\nu = 10^{10}$ Hz and $T_{\rm HI}$ =20000 K; here $x = -0.067$, and scattering occurs almost entirely off of hydrogen atoms whose velocities are such that the photon frequency in

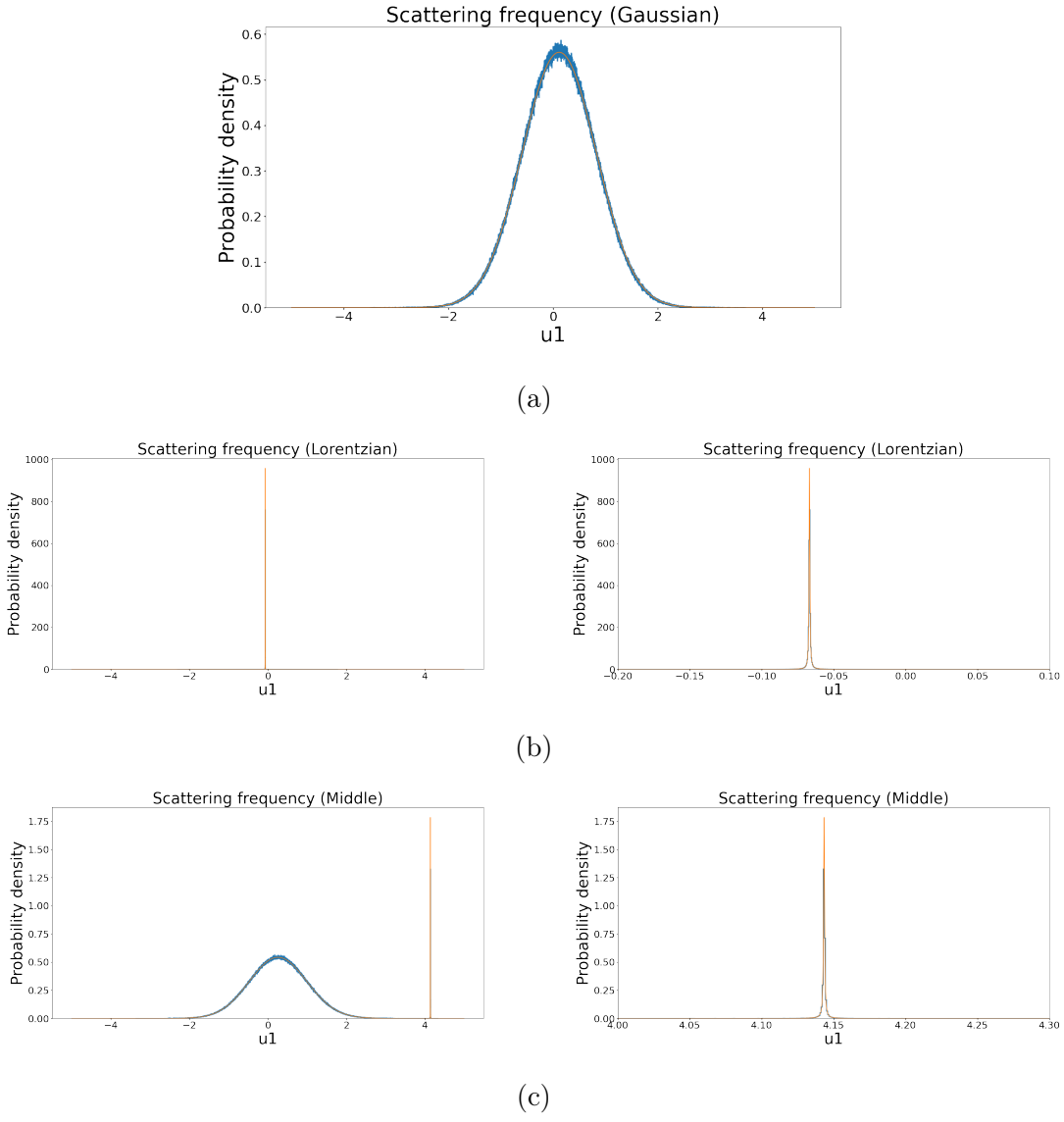

Figure 6: *Blue curves*: The simulated probability density of atomic velocity u_1 for (a) the Gaussian limit; (b) the Lorentzian limit; and (c) an intermediate bimodal case. *Orange curves*: The analytic prediction for the probability distribution.

the atom frame is on the Lyman-α resonance. The result is a Lorentzian distribution of width a centered at $u_1 = x$. Figure 6c shows an intermediate case with $\Delta\nu = -5 \times 10^{11}$ Hz and $T_{\rm HI}$ =13000 K; here $x = 4.143$ and it has a bimodal distribution, with one broad peak neat $u_1 \approx 0 \pm 1$ (where most of the H I atoms are located) and a narrow peak at $u_1 \approx x \pm a$ (where the photon is resonant in the atom frame). In this

test, about 79.73% of the photon is in the broad peak, 0.04% of the photon is in the narrow peak, and 20.23% is distributed between $u_1 \approx$ -3.358 to $u_1 \approx 4.334$. I set both the initial direction and initial polarization to 0 for all three cases, and run 10^7 photons for each case. The orange lines are the theoretical distribution according to Lee [35] (notice that the Voigt function here should be divided by $\sqrt{\pi}$ to be normalized to 1), and they are consistent with the simulation results.

4.4 Scattering direction and polarization

Additional tests for the scattering process were done to ensure given an initial direction and polarization, the probability distribution of scattering direction matched theoretical expectations. For initial $\mu_{\rm i} = 0$ and polarization $p_{\rm i} = 0$ and large x (which results in pure dipole scattering, $E_1 = 1$), it sees from Eq. (3.18) that

$$\mathrm{P}(\boldsymbol{n}, \mathrm{NS}|\boldsymbol{n'}, p') = \frac{3}{16\pi}(\cos^2\psi_{\mathrm{NS,NS}} + \cos^2\psi_{\mathrm{NS,EW}}), \tag{4.1}$$

where $\cos\psi_{NS,NS} = \sin\theta$ and $\cos\psi_{\mathrm{NS,EW}} = -\cos\theta\sin\zeta$. Using Eq. (3.19), it knows

$$\mathrm{P}(\boldsymbol{n}, \mathrm{EW}|\boldsymbol{n'}, p') = \frac{3}{16\pi}[\cos^2\psi_{\mathrm{EW,NS}} + \cos^2\psi_{\mathrm{EW,EW}}] \tag{4.2}$$

but $\cos\psi_{\mathrm{EW,EW}} = 0$, so it can see that after integrating over all ζ from 0 to 2π that

$$\mathrm{P}(\boldsymbol{n}|\boldsymbol{n'} = \boldsymbol{0}, p' = 0) = \frac{3}{16}(3 - \mu^2). \tag{4.3}$$

This matched our simulation results as seen in Fig. 7. Using similar arguments for the isotropic case ($E_1 = 0$), it can show that $\mathrm{P}(\boldsymbol{n}|\boldsymbol{n'} = \boldsymbol{0}, p' = 0) = \frac{1}{2}$. For small x case, the scattering type is mixed with about 2/3 pure isotropic and 1/3 pure dipole, thus, when the initial $\mu_{\rm i} = 0$ and initial polarization $p_{\rm i} = 0$, the probability density is

$$\mathrm{P}(\boldsymbol{n}|\boldsymbol{n'} = \boldsymbol{0}, p' = 0) = \frac{2}{3} \times \frac{1}{2} + \frac{1}{3} \times \frac{3}{16}(3 - \mu^2) = \frac{1}{3} + \frac{3 - \mu^2}{16}, \tag{4.4}$$

which also matches the results of the simulation. Other tests with analytic solutions were run with $p_{\rm i} = 1, -1$ with pure dipole and mixed conditions, with results shown in Table 1. All simulated distributions had consistent results with the analytic distributions.

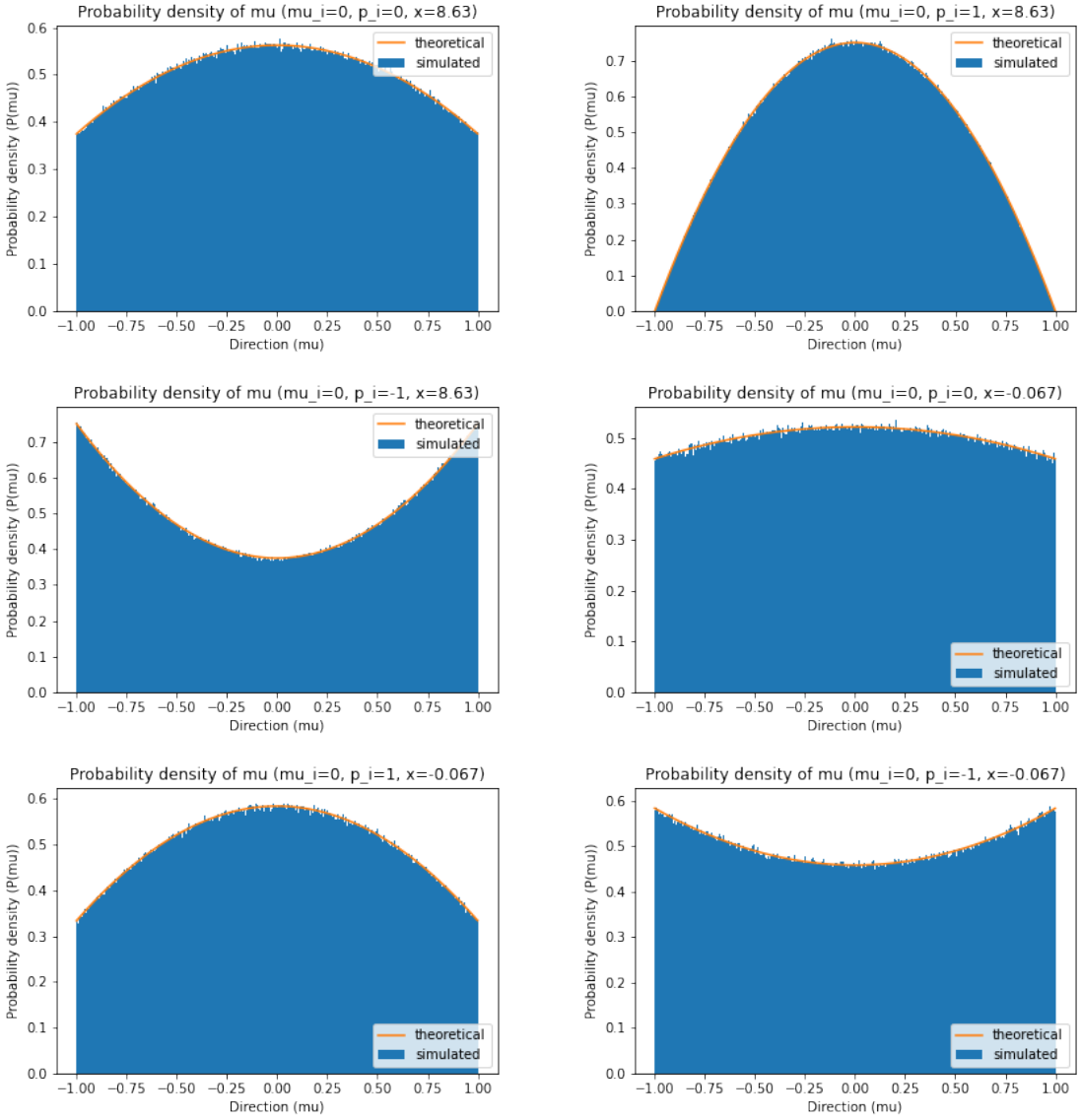

Figure 7: Simulated and fitted results for the probability density of a photon being emitted in some direction μ. All photons are initially traveling along $\mu_{\mathrm{i}} = 0$. The initial polarization values differ in the plots, and the figures represent the different x, which also represents the scattering type.

scattering type	$p_\mathrm{i} = -1$	$p_\mathrm{i} = 0$	$p_\mathrm{i} = 1$
mixed ($E_1 = \frac{1}{3}$; Doppler core)	$\frac{1}{3} + \frac{1}{8}(1+\mu^2)$	$\frac{1}{3} + \frac{1}{16}(3-\mu^2)$	$\frac{1}{3} + \frac{1}{4}(1-\mu^2)$
pure dipole ($E_1 = 1$; damping wing)	$\frac{3}{8}(1+\mu^2)$	$\frac{3}{16}(3-\mu^2)$	$\frac{3}{4}(1-\mu^2)$

Table 1: Analytical results for the probability density of a photon being emitted in some direction μ. All photons are initially traveling along $\mu_\mathrm{i} = 0$. The initial polarization values differ in the columns, and the rows represent the different scattering law possibilities.

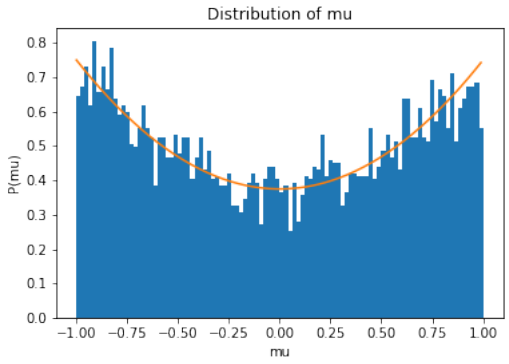

Figure 8: Distribution of scattering direction for the optical thin case.

4.5 Optically Thin Limit

To test scattering along the front, I inject photons into the neutral side with $n_\mathrm{HI} = 1.37 \times 10^{-5}\,\mathrm{cm}^{-3}$ (neutral fraction of hydrogen is 0.999) in the damping wings. Here I set the photons initially to $p = 0$ (unpolarized) and $\mu = 1$ (propagating directly toward the neutral side of the front) with $\Delta\nu = -8.8 \times 10^{12}$ Hz. Then I can calculate the optical depth before the photon exits the frequency grid by taking the Sobolev optical depth [36] and multiplying it by the fraction of the line profile swept out (the damping wing profile is $\propto \Delta\nu^{-2}$ and can be analytically integrated):

$$\tau = \frac{3A^2 n_\mathrm{HI} \lambda_\mathrm{center}^3}{32\pi^3 H} \left(\frac{1}{|\Delta\nu_\mathrm{ini}|} - \frac{1}{|\Delta\nu_\mathrm{limit}|} \right). \tag{4.5}$$

For this case, I find $\tau = 0.0555$; then the probability of not scattering is $e^{-\tau} = 0.9460$ and the probability of scattering is 0.0540. I run 10^5 photons and get 5340 photons

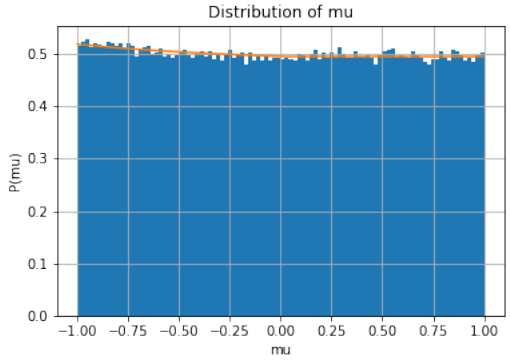

Figure 9: Distribution of scattering direction for the optical thick case.

scattering, the probability of scattering is 0.0534 ± 0.0007 (1σ binomial error), which is consistent with expectations. For the scattering photons, I expect pure dipole scattering since they are in the damping wing, and it should get $\mathrm{P}(\mu) = \frac{3}{8}(1+\mu^2)$. Figure 8 shows the distribution of scattering photons and corresponds to this expectation.

4.6 Optically Thick Limit

Finally, I want to test the optical thick limit. Here I set all other settings the same as the optical thin case, but $\Delta\nu = 8.8 \times 10^{12}$ Hz. Since the photons start from the blue side of the line and then redshift toward the line center, I expect nearly all of the photons to scatter. Most of the photons will scatter many times in the neutral region and isotropize, so they approach a uniform distribution of μ with $\mathrm{P}(\mu) = 1/2$. It will have a slight excess of photons with $\mu \approx -1$ as they may be single scatterings that go back and enter the ionized region before they redshift into the line center. I run 5×10^5 photons, in this case, to reduce the noise to signal ratio, and after excluding the single-scatterings case, I get the result shown in Figure 9, which is corresponding to our expectation. In this test, the theoretical distribution would be

$$P(\mu) = \frac{1}{2}(1 - P_{\mathrm{all}}) + \begin{cases} P_{1\,\mathrm{scatter}}(\mu) & \mu < 0 \\ 0 & \mu \geq 0, \end{cases} \tag{4.6}$$

where

$$P_{1\,\mathrm{scatter}}(\mu) = \frac{3}{8}(1+\mu^2)\,\tau \int_0^{\frac{1}{1-1/\mu}} e^{-\tau\,(1-1/\mu)}\,\frac{x}{[1-(1-1/\mu)\,x]\,(1-x)}dx, \tag{4.7}$$

I have defined $P_{\mathrm{all}} = \int_{-1}^{0} P_{1\,\mathrm{scatter}}(\mu)\,d\mu$, and τ is the same as in Eq. (4.5).

5 Parameters from Coeval Cubes

As all parts of the model satisfy my expectations, I want to extend this model to coeval cubes generated by the 21cmFAST tool [37, 38]. To apply for other ionization fronts, it needs redshift z, blackbody temperature T_{bb}, front velocity U and number density of neutral hydrogen n_{H}. In this case, I fix the redshift at 8. For 21cmFAST, $T_{\mathrm{bb}} = 47834.5 \pm 211.7$ K is fixed, then I only need to figure out U and n_{H}.

5.1 Number Density of Neutral Hydrogen

21cmFAST doesn't save number density directly, but it does store the matter overdensity data, so I could calculate the hydrogen number density by

$$n_{\mathrm{H}} = \bar{n}_{\mathrm{H}}(1+\delta_{\mathrm{b}}) \approx \frac{\Omega_{\mathrm{b}}(z) Y_{\mathrm{H}} \rho_{\mathrm{crit}}}{m_{\mathrm{H}}}(1+\delta_{\mathrm{m}}). \tag{5.1}$$

Ω_{b} is the baryon abundance at the redshift we investigate, with $\Omega_{\mathrm{b}} = \Omega_0(1+z)^3$. $Y_{\mathrm{H}} = 0.76$ is the hydrogen fraction. $\rho_{\mathrm{crit}} = 1.878 \times 10^{-29}\mathrm{g\,cm^{-3}}$ is the critical density, m_{H} is the hydrogen atom mass and δ_{m} is the matter overdensity that could be extracted from simulation box. Then I can calculate the number density by giving redshift z and the simulation result from 21cmFAST.

5.2 Front Velocity

Finally, I want the front velocity U, where the front velocity satisfies the following equation:

$$\frac{n_{\mathrm{H}}(1+f_{\mathrm{He}})U}{1-U/c} = \int_{I_{\mathrm{H}}/h}^{\infty} d\nu \frac{F_\nu^{\mathrm{inc}}}{h\nu} = \frac{\Gamma_{\mathrm{HI}}(\mathrm{ionized\,side})}{\bar{\sigma}_{\mathrm{HI}}}. \tag{5.2}$$

$f_{\rm He} = 0.079$ is the helium fraction, c is the speed of light, $\Gamma_{\rm HI}$ is the photoionization rate, and $\bar{\sigma}_{\rm HI}$ is the mean Thompson scattering cross section. $\Gamma_{\rm HI}$ is stored in 21cmFAST result boxes, and $\bar{\sigma}_{\rm HI}$ can be calculated from

$$\bar{\sigma}_{\rm HI} = \frac{\int_{I_{\rm H}/h}^{4I_{\rm H}/h} d\nu F_\nu^{\rm inc} \sigma_{\rm HI}(\nu)/h\nu}{\int_{I_{\rm H}/h}^{4I_{\rm H}/h} d\nu F_\nu^{\rm inc}/h\nu}, \tag{5.3}$$

where $I_{\rm H} = 13.6$ eV is ionization energy of hydrogen, h is Planck constant, and

$$F_\nu^{\rm inc} = \frac{2h\nu^3}{c^2\left(e^{h\nu/kT} - 1\right)h\nu}, \tag{5.4}$$

$$\sigma_{\rm HI}(\nu) = \sigma_0 (\frac{\nu_0}{\nu})^4 \frac{e^{4(1-\arctan(\nu/\nu_0-1))/(\nu/\nu_0-1)}}{1 - e^{-2\pi/(\nu/\nu_0-1)}}. \tag{5.5}$$

After integrating the ν, $\bar{\sigma}_{\rm HI}$ is only depend on $T_{\rm bb}$. Thus, U is depend on $T_{\rm bb}$, $\Gamma_{\rm HI}$, $n_{\rm H}$, which I can get either direct from the 21cmFAST boxes or from previous calculating.

6 Discussion

With the model presented in this paper, I can calculate the total and polarized intensity of the Lyman-α emission from the ionization front as a function of the basic physical inputs: the incident radiation spectrum; the gas density; and the viewing geometry of the observer. The model contains a detailed treatment of the physics of the ionization front, including (i) H and He ionization structure, including tracking the attenuation of each frequency bin in the incident spectrum; (ii) thermal evolution and collisional Lyman-α production rates for a multi-temperature plasma; (iii) Monte Carlo treatment of the photon propagation through the ionization front, including redshifting and scattering with frequency distribution; and (iv) tracking of the photon polarization, including the joint polarization-angular-frequency dependence of the scattering cross section. I have constructed a grid of models and explored the dependence of the polarized intensity on the model parameters.

The remaining goal is to go from the emergent polarized intensities computed from these grids to the observable power spectrum of Lyman-α emission from the

ionization fronts. Aside from the extraction of needed parameters I have done in this paper, this requires me to run a simulation of reionization in a cosmological volume, identify the ionization fronts, interpolate from our grid to compute the Lyman-α polarization in each cell, and finally run a power spectrum estimator on the simulated box.

References

[1] P. R. Upton Sanderbeck, A. D'Aloisio and M. J. McQuinn, *Models of the thermal evolution of the intergalactic medium after reionization*, **460** (Aug., 2016) 1885–1897, [1511.05992].

[2] V. Iršič, M. Viel, M. G. Haehnelt, J. S. Bolton, S. Cristiani, G. D. Becker et al., *New constraints on the free-streaming of warm dark matter from intermediate and small scale Lyman-α forest data*, **96** (July, 2017) 023522, [1702.01764].

[3] N. Y. Gnedin and L. Hui, *Probing the Universe with the Lyalpha forest - I. Hydrodynamics of the low-density intergalactic medium*, **296** (May, 1998) 44–55, [astro-ph/9706219].

[4] P. Montero-Camacho, C. M. Hirata, P. Martini and K. Honscheid, *Impact of inhomogeneous reionization on the Lyman-α forest*, **487** (July, 2019) 1047–1056, [1902.02892].

[5] A. Liu, J. R. Pritchard, R. Allison, A. R. Parsons, U. Seljak and B. D. Sherwin, *Eliminating the optical depth nuisance from the CMB with 21 cm cosmology*, **93** (Feb., 2016) 043013, [1509.08463].

[6] B. E. Robertson, R. S. Ellis, S. R. Furlanetto and J. S. Dunlop, *Cosmic Reionization and Early Star-forming Galaxies: A Joint Analysis of New Constraints from Planck and the Hubble Space Telescope*, **802** (Apr., 2015) L19, [1502.02024].

[7] S. L. Finkelstein, J. Ryan, Russell E., C. Papovich, M. Dickinson, M. Song, R. S. Somerville et al., *The Evolution of the Galaxy Rest-frame Ultraviolet Luminosity Function over the First Two Billion Years*, **810** (Sept., 2015) 71, [1410.5439].

[8] S. L. Finkelstein, A. D'Aloisio, J.-P. Paardekooper, J. Ryan, Russell, P. Behroozi, K. Finlator et al., *Conditions for Reionizing the Universe with a Low Galaxy Ionizing Photon Escape Fraction*, **879** (July, 2019) 36, [1902.02792].

[9] J. S. Bullock, A. V. Kravtsov and D. H. Weinberg, *Reionization and the Abundance of Galactic Satellites*, **539** (Aug., 2000) 517–521, [astro-ph/0002214].

[10] E. D. Kovetz, M. P. Viero, A. Lidz, L. Newburgh, M. Rahman, E. Switzer et al., *Line-Intensity Mapping: 2017 Status Report*, *arXiv e-prints* (Sept., 2017) arXiv:1709.09066, [1709.09066].

[11] Planck Collaboration, N. Aghanim, Y. Akrami, M. Ashdown, J. Aumont, C. Baccigalupi et al., *Planck 2018 results. VI. Cosmological parameters*, **641** (Sept., 2020) A6, [1807.06209].

[12] J. E. Gunn and B. A. Peterson, *On the Density of Neutral Hydrogen in Intergalactic Space.*, **142** (Nov., 1965) 1633–1636.

[13] X. Fan, V. K. Narayanan, R. H. Lupton, M. A. Strauss, G. R. Knapp, R. H. Becker et al., *A Survey of z>5.8 Quasars in the Sloan Digital Sky Survey. I. Discovery of Three New Quasars and the Spatial Density of Luminous Quasars at z~6*, **122** (Dec., 2001) 2833–2849, [astro-ph/0108063].

[14] R. H. Becker, X. Fan, R. L. White, M. A. Strauss, V. K. Narayanan, R. H. Lupton et al., *Evidence for Reionization at z~6: Detection of a Gunn-Peterson Trough in a z=6.28 Quasar*, **122** (Dec., 2001) 2850–2857, [astro-ph/0108097].

[15] X. Fan, C. L. Carilli and B. Keating, *Observational Constraints on Cosmic Reionization*, **44** (Sept., 2006) 415–462, [astro-ph/0602375].

[16] S. Malhotra and J. E. Rhoads, *Luminosity Functions of Lyα Emitters at Redshifts z=6.5 and z=5.7: Evidence against Reionization at z<=6.5*, **617** (Dec., 2004) L5–L8, [astro-ph/0407408].

[17] Z.-Y. Zheng, J. Wang, J. Rhoads, L. Infante, S. Malhotra, W. Hu et al., *First Results from the Lyman Alpha Galaxies in the Epoch of Reionization (LAGER) Survey: Cosmological Reionization at z ~ 7*, **842** (June, 2017) L22, [1703.02985].

[18] K. Ota, M. Iye, N. Kashikawa, A. Konno, F. Nakata, T. Totani et al., *A New*

*Constraint on Reionization from the Evolution of the Lyα Luminosity Function at z ∼ 6-7 Probed by a Deep Census of z = 7.0 Lyα Emitter Candidates to 0.3L **, **844** (July, 2017) 85, [1703.02501].

[19] A. Konno, M. Ouchi, T. Shibuya, Y. Ono, K. Shimasaku, Y. Taniguchi et al., *SILVERRUSH. IV. Lyα luminosity functions at z = 5.7 and 6.6 studied with ˜1300 Lyα emitters on the 14-21 deg^2 sky*, **70** (Jan., 2018) S16, [1705.01222].

[20] P. Madau, A. Meiksin and M. J. Rees, *21 Centimeter Tomography of the Intergalactic Medium at High Redshift*, **475** (Feb., 1997) 429–444, [astro-ph/9608010].

[21] P. A. Shaver, R. A. Windhorst, P. Madau and A. G. de Bruyn, *Can the reionization epoch be detected as a global signature in the cosmic background?*, **345** (May, 1999) 380–390, [astro-ph/9901320].

[22] A. Loeb and G. B. Rybicki, *Scattered Lyα Radiation around Sources before Cosmological Reionization*, **524** (Oct., 1999) 527–535, [astro-ph/9902180].

[23] M. Dijkstra and A. Loeb, *The polarization of scattered Lyα radiation around high-redshift galaxies*, **386** (May, 2008) 492–504, [0711.2312].

[24] L. Mas-Ribas and T.-C. Chang, *Lyman-α polarization intensity mapping*, **101** (Apr., 2020) 083032, [2002.04107].

[25] J. Miralda-Escudé and M. J. Rees, *Reionization and thermal evolution of a photoionized intergalactic medium.*, **266** (Jan., 1994) 343–352.

[26] S. Cantalupo, C. Porciani and S. J. Lilly, *Mapping Neutral Hydrogen during Reionization with the Lyα Emission from Quasar Ionization Fronts*, **672** (Jan., 2008) 48–58, [0709.0654].

[27] C. Zeng and C. M. Hirata, *Nonequilibrium Temperature Evolution of Ionization Fronts during the Epoch of Reionization*, **906** (Jan., 2021) 124, [2007.02940].

[28] Y. Ali-Haïmoud and C. M. Hirata, *HyRec: A fast and highly accurate primordial hydrogen and helium recombination code*, **83** (Feb., 2011) 043513, [1011.3758].

[29] K. M. Aggarwal, *Excitation rate coefficients form the ground state of atomic hydrogen to the N = 2 and N = 3 levels*, **202** (Jan., 1983) 15P–20P.

[30] C. M. Hirata, *Wouthuysen-Field coupling strength and application to high-redshift 21-cm radiation*, **367** (Mar., 2006) 259–274, [astro-ph/0507102].

[31] J. R. Pritchard and S. R. Furlanetto, *Descending from on high: Lyman-series cascades and spin-kinetic temperature coupling in the 21-cm line*, **367** (Apr., 2006) 1057–1066, [astro-ph/0508381].

[32] I. Harris, Daniel L., *On the Line-Absorption Coefficient due to Doppler Effect and Damping.*, **108** (July, 1948) 112.

[33] J. S. Lee, *Refined Monte-Carlo Method for Simulating Angle-Dependent Partial Frequency Redistributions*, **255** (Apr., 1982) 303.

[34] S. Chandrasekhar, *Radiative transfer*. 1960.

[35] J. S. Lee, *Simulation of emission frequencies from angle-dependent partial frequency redistributions.*, **218** (Dec., 1977) 857–865.

[36] V. V. Sobolev, *Moving envelopes of stars*. 1960.

[37] S. G. Murray, B. Greig, A. Mesinger, J. B. Muñoz, Y. Qin, J. Park et al., *21cmfast v3: A python-integrated c code for generating 3d realizations of the cosmic 21cm signal.*, *Journal of Open Source Software* **5** (2020) 2582.

[38] A. Mesinger, S. Furlanetto and R. Cen, *21cmfast: a fast, seminumerical simulation of the high-redshift*
21-cm signal, *Monthly Notices of the Royal Astronomical Society* **411** (02, 2011) 955–972, [https://academic.oup.com/mnras/article-pdf/411/2/955/4099991/mnras0411-0955.pdf].